



OPEN

Pre-seizure state identified by diffuse optical tomography

SUBJECT AREAS:

APPLIED PHYSICS

NEUROSCIENCE

BIOMEDICAL ENGINEERING

APPLIED OPTICS

Tao Zhang¹, Junli Zhou², Ruixin Jiang¹, Hao Yang¹, Paul R. Carney^{1,2,3,4} & Huabei Jiang¹

¹J. Crayton Pruitt Family Department of Biomedical Engineering, University of Florida Gainesville, FL 32611, USA, ²Department of Pediatrics, University of Florida Gainesville, FL 32611, USA, ³Department of Neurology, University of Florida Gainesville, FL 32611, USA, ⁴Department of Neuroscience, University of Florida Gainesville, FL 32611, USA.

Received
20 May 2013

Accepted
30 December 2013

Published
21 January 2014

Correspondence and
requests for materials
should be addressed to

H.B.J. (hjiang@bme.
ufl.edu) or P.R.C.
(carneypr@peds.ufl.
edu)

In epilepsy it has been challenging to detect early changes in brain activity that occurs prior to seizure onset and to map their origin and evolution for possible intervention. Here we demonstrate using a rat model of generalized epilepsy that diffuse optical tomography (DOT) provides a unique functional neuroimaging modality for noninvasively and continuously tracking such brain activities with high spatiotemporal resolution. We detected early hemodynamic responses with heterogeneous patterns, along with intracranial electroencephalogram gamma power changes, several minutes preceding the electroencephalographic seizure onset, supporting the presence of a “pre-seizure” state. We also observed the decoupling between local hemodynamic and neural activities. We found widespread hemodynamic changes evolving from local regions of the bilateral cortex and thalamus to the entire brain, indicating that the onset of generalized seizures may originate locally rather than diffusely. Together, these findings suggest DOT represents a powerful tool for mapping early seizure onset and propagation pathways.

Epilepsy is one of the most common and devastating neurologic diseases affecting over 2.5 M Americans. Seizure control with antiepileptic drugs (AEDs) has been proven to decrease morbidity and mortality and remains the only treatment option for the majority of patients. Nevertheless, despite progress in antiepileptic drug development, at least 30% of all epilepsy cases remain resistant to current therapeutics^{1,2}. For patients without complete seizure control, the sudden, unforeseen occurrence represents one of the most debilitating aspects of epilepsy. Amongst the types of epileptic seizures, generalized tonic-clonic seizures are the most dangerous form, which has the potential to cause severe injuries or even death^{3,4}. However, by providing appropriate and timely prevention, the risk factor can be significantly reduced⁵.

In the absence of completely controlling a patient's epilepsy, predicting seizures is an important goal of clinical management and treatment. A question of fundamental importance to seizure prediction is to better understand the brain dynamics during the transition from interictal to the seizure state. A promising and widely studied candidate for seizure precursor is high frequency oscillations (HFOs). Recent studies have shown that HFOs occur in advance of impending seizures indicating its strong relationship with the seizure onset zone^{6,7}.

Most seizure prediction methods are based on mathematically extracting specific features from multiscale intracranial electroencephalogram (IEEG) recordings⁸. Although studies have focused on prospectively testing these methods, no study to date has yet confirmed the ability of any method to predict seizures better than random⁹. Invasive intracranial electrodes are required to detect oscillations generated in very localized or deep brain regions. Owing to the IEEG's insufficient spatial sampling, a barrier to obtaining better seizure predictive rates has been the inconsistency in identifying the earliest changes prior to seizure onset. A deeper understanding of the regional interactions at the beginning and during the evolution of a seizure may help identify the earliest seizure susceptible brain regions^{10–12}.

To advance our knowledge about seizure initiation, functional brain imaging techniques like single-photon emission computed tomography (SPECT) and functional magnetic resonance imaging (fMRI) are used to answer questions regarding whether so-called ‘preictal states’ can be distinguished from the ictal period and the functional networks in the brain responsible for seizure generation. With SPECT's ability to capture a “snapshot” of cerebral blood flow, studies in^{13,14} observed cerebral blood flow (CBF) increases a few seconds to several minutes preceding clinical electroencephalographic (EEG) seizure onset in temporal lobe partial seizures. With fMRI's high spatial resolution and its combination with EEG, fMRI studies recently reported that blood-oxygen-level-dependent (BOLD) changes occur minutes prior to seizure onset, either in animals or in humans^{4,15,16}. However, due to relatively low temporal resolution and lack of portability, such techniques are not suitable for rigorous



statistical seizure prediction analyses, which often require continuous longtime monitoring of the period prior to, during, and after seizures, as well as the continuous interictal state⁸.

Taking advantage of the near-infrared (NIR) window in tissue, optical imaging brings new opportunities to brain studies. Changes in optical spectroscopic properties of brain tissue are often correlated with changes in neuronal activity¹⁷. Activity evoked optical spectroscopic changes measured in the brain are most likely generated by changes in cerebral hemodynamics. Therefore, such optical properties changes are also the hallmarks of seizure generation and the spread of ictal neural activity. With the ability to provide excellent brain surface maps, intrinsic optical signal (IOS) methodologies have been used in animal models to study seizure foci localization, propagation, and neurovascular coupling^{18,19}. It was also found in an intraoperative procedure that local change of intrinsic signal preceded the seizure onset by approximately 20 seconds²⁰. Functional near-infrared spectroscopy (fNIRS) has also been applied to investigate epileptic seizures^{21,22} and other brain disorders²³, especially in daily clinical use due to its non-invasive and portable merits. A major limitation of IOS and fNIRS is that each fails to provide much depth information. However, depth information can be obtained by using tomographic reconstruction methods such as diffuse optical tomography (DOT)^{24,25}. Here, multispectral NIR light is sequentially delivered to the tissue at multiple locations and the diffusely scattered light are measured at multiple positions along the scalp, which are used to reconstruct the spatial distribution of tissue absorption and scattering coefficients at each wavelength through a light propagation model in tissue. The images of absorption spectra are then used to derive the images of functional parameters such as oxy- and deoxy-hemoglobin²⁶. Indeed, DOT offers sub millimeter resolution within centimeter thick tissue²⁷. In the area of neuroimaging, DOT has been applied to study hemodynamic response to motor and visual stimulations in several cortical areas^{28,29}, and to quantify cerebral perfusion³⁰ and blood flow³¹, both in humans and small animals. These studies show that DOT is capable of detecting hemodynamic responses spatially equivalent to fMRI.

The primary goal of this study was to identify hemodynamics prior to and during seizures in a rat model of generalized epilepsy. Our fast three-dimensional (3-D) DOT system, combined with simultaneous IEEG recordings, allowed us to track both changes in hemodynamics and local field potentials (multiunit activity) throughout the brain during Pentylentetrazol (PTZ)-induced generalized tonic-clonic seizures in rats. We found that hemodynamic changes precede seizure onset by ~1 to 3 minutes, and that seizure zones initiated from a regional onset and then distributed to the entire brain. We also observed the decoupling between local field potentials and hemodynamic changes, accompanied by concurrent scattering changes. For the first time, the whole process of generalized tonic-clonic seizures was recorded *in vivo*, including the interictal state, the preictal transition state, and the ictal onset state. Our findings suggest that a pre-seizure state can be detected with optical imaging and the “generalized” seizures originate from a regional (focal) onset zone.

Results

Hemodynamic responses elicited during generalized PTZ-induced seizures. Generalized tonic-clonic seizures and corresponding hemodynamic changes were observed in 9/9 seizure rats elicited by i.p. PTZ. Time courses of the EEG gamma power and hemodynamic changes for all nine experiments are shown in supplementary Fig. S1. A representative (rat #1) co-located neural and hemodynamic response from left primary motor (M1) is shown in Fig. 1. Time series data of local concentration of oxy- [HbO₂] and deoxy-hemoglobin [Hb_R] were extracted from the same location as the IEEG recording. Continuous spike and wave discharges occurred abruptly within 4 minutes after i.p. PTZ (Fig. 1a). Power spectrum density changes can also be seen on the time-frequency analysis

(Fig. 1b). Significant hemodynamic changes (t-test, $p < 0.05$) are displayed in Fig. 1c. During the resting state, [HbO₂] and [Hb_R] showed no significant changes, only with little fluctuations around their resting state values of ~30 μM and ~10 μM , respectively. Chromophore concentrations were calculated from the reconstructed absorption coefficients distribution from three wavelengths. After PTZ injection, a 15 μM decrease of [HbO₂], and a corresponding 3 μM increase of [Hb_R] was observed. The hemodynamic responses were comprised of a large change of [HbO₂] with a relatively smaller change of [Hb_R]. These findings are consistent with other studies of epilepsy using optical methods like NIRS³², diffuse optical imaging (DOI)³³, where [HbO₂] and the concentration of total hemoglobin [HbT] followed similar trends accompanying by a small variation of [Hb_R]. Interestingly, IEEG power increase (Fig. 1b) in the fast gamma frequency range (80 ~ 120 Hz) was observed before seizure onset (Pearson Correlation: 0.89) with the hemodynamic change. Similar phenomenon has been reported before by comparing optical intrinsic signals and local field potentials (LFPs)³⁴. In the age-matched sham saline control experiments, no detectable IEEG spikes or significant hemodynamic changes were observed (Fig. 1d–f).

Hemodynamic changes precede IEEG spikes. We also found that hemodynamic changes began before seizure onset in 9/9 rats, although the pre-seizure time (lead time) for observed changes varied for each seizure. A statistics of such neural and hemodynamic changes for all nine rats experiments is listed in the supplementary Table S1. The lead time represents the interval between the moment when the first significant hemodynamic changes (t-test, $p < 0.05$) appear in any voxel and the electrographic onset time. A representative result from rat #2 is shown in Fig. 2. Locations of two regions of interests (ROIs), one from the motor cortex and the other from temple lobe are shown in a coronal slice (Fig. 2a left). By tracking the change of [HbT], whereas a significant hemodynamic decrease (t-test, $p < 0.05$) in ROI1 (Fig. 2c, top) and increase in ROI2 (Fig. 2c, bottom) occurred about 20 seconds after PTZ injection, the IEEG (recorded at ROI1) seizure onset began 1 minute after PTZ injection (Fig. 2b). The gamma power, having a tight relationship with [HbT] (Pearson correlation, 0.85), started to change almost at the same time as [HbT] (Fig. 2b). In Fig. 2d, the activation maps of [HbT], superimposed on the MRI template, shows the evolution of hemodynamic distribution in the whole brain. We use cool or warm color to specify [HbT] decreasing or [HbT] increasing. [HbT] started to change in the preictal period and remained relatively stable after tonic-clonic seizure onset. In Fig. 2e, we compare the results from all experiments ($n = 9$) of the time lengths between PTZ injection and occurrence of electroencephalographic seizure onset, significant gamma power changes and significant hemodynamic changes. On average, the hemodynamic change, similar to the gamma power change, leads IEEG seizure onset ~80 seconds.

Decoupling of IEEG and hemodynamic changes. Both neural (local field potentials) and hemodynamic activity (HbT, HbO₂, and Hb_R) from bilateral primary motor cortex (M1), bilateral somatosensory cortex trunk region (S1Tr), bilateral hind limb primary somatosensory cortex (SIHL), and bilateral anterior thalamic regions, were studied using simultaneous IEEG and DOT (Fig. 3a). Results of seizure experiment from rat #2 are shown here. We note that a local dissociation between hemodynamic changes and local field potentials (left M1, S1Tr, Thalamus and right M1) during the preictal period was observed, suggesting a lag between measurable local neural activity (gamma power) and local hemodynamics relative to seizure onset. Moreover, changes of reconstructed local scattering coefficients, as much as 0.3 mm^{-1} compared to the resting state value of ~1.3 mm^{-1} , occurred concurrently with the hemodynamic changes. These findings further suggest that changes in

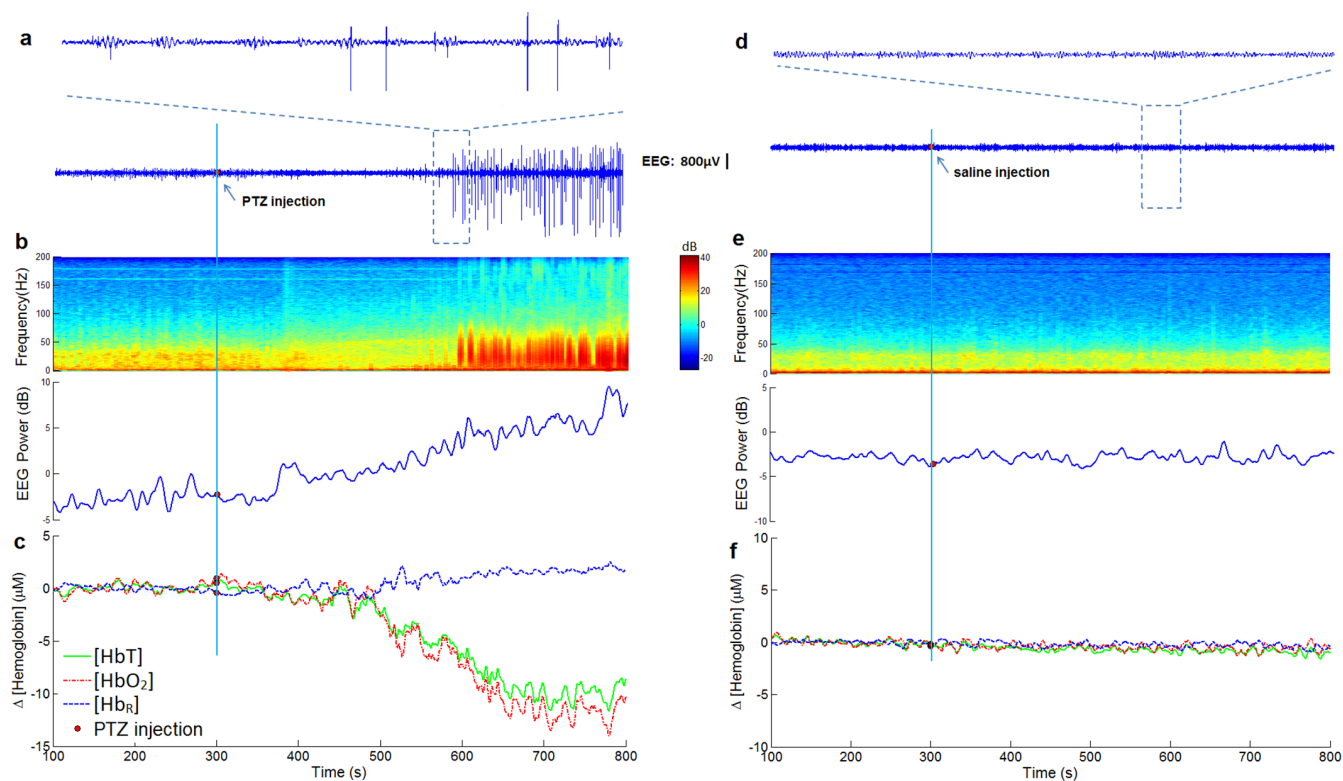


Figure 1 | Neural and hemodynamic responses elicited during generalized PTZ-induced seizures. (a), (b) and (c) are results from seizure experiments of rat #1 with PTZ injection sharing a same time line; (d), (e) and (f) are results from control experiments with saline injection sharing a same time line. The time point of PTZ or saline injection is indicated by the red dots. EEG and hemodynamic traces are picked up at the same location in left M1. (a) Seizure spikes were observed from IIEG recordings after PTZ injection. (b) Obvious power spectral density changes EEG power increase in the fast gamma frequency range (80 ~ 120 Hz) were seen in IIEG time-frequency analysis during seizures. (c) Hemodynamic responses of [HbT], [HbO₂] and [Hb_R] from left M1 induced by PTZ. (d) IIEG recordings in the control experiment. (e) IIEG time-frequency analysis for control experiment. (f) No obvious hemodynamic changes were observed in the control experiments.

hemodynamic activity alter tissue scattering properties, not readily visible with concurrent IIEG.

We also observed early gamma power increase during the preictal period from most IIEG electrodes. This may indicate an early buildup of synchrony as a preparation for the generalized seizure onset. During seizures, we can see that seizure spikes with larger intensities (left side) tend to accompany with larger hemodynamic changes, suggesting a correspondence between local neural and hemodynamic activities as seizures progress into ictal stage. Besides, despite the existence of seizure spikes, the hemodynamic changes in S1HL (left and right) and S1Tr (right) have neither obvious increasing nor decreasing trend in such areas. However, large fluctuations in these areas are still notable, indicating that the hemodynamic activities are not as uniformly distributed as neural activities during the “generalized” seizures.

Evolution and distribution of seizures. Amongst all nine rats, we selected three experiments from rat #2, #3 and #4 with increasing seizure intensities to show the overall seizure evolutions through the whole brain. Fig. 4a gives the positions of five coronal slices selected for activation maps. The coordinates of these slices range from -5 mm to 5 mm relative to bregma. IIEG recordings and statistical activation maps that depict [HbT] increases (warm colors) and decreases (cool colors) compared with the baseline DOT images (t-test, $p < 0.05$), are shown in Fig. 4b–d.

Seizures activities shown in Fig. 4c were more robust than that depicted in Fig. 4b in term of amplitude and frequency of spikes. Accordingly, larger hemodynamic changes, positive or negative activations were observed in Fig. 4c compared to changes in Fig. 4b. Amongst seizures Fig. 4d shows a high grade seizure in which

continuous and high amplitude polyspikes were seen with concomitant behavioral changes twitching limbs and stretching its body even under anesthesia. Furthermore, at the peaks during the preictal period, the activation regions in Fig. 4b,c remained relatively stable during the ictal period. Conversely, in Fig. 4d, as IIEG spike pattern changed strongly during ictal period, the activation regions changed accordingly. We observed large hypoperfusion area in Fig. 4d, possibly due to the excessive energy consumption of the electrical activities during the fierce seizures onset.

Discussion

Multispectral DOT was used to investigate seizure dynamics in a rat PTZ seizure model. Changes in local and global hemodynamics and local field potentials were identified during seizure initiation and propagation. Early hemodynamic changes with concurrent gamma power increase were found several minutes prior to seizure onset supporting the presence of a preictal state. The early changes in optical scattering property offer a possible explanation for the decoupling of local field potentials from early hemodynamic changes during the preictal stage. We also found that generalized seizures initiate with focal hemodynamic changes and subsequently evolve to widespread changes throughout the brain.

There is general agreement that despite pharmacological, neuro-modulation, dietary, and surgical advances in the treatment of chronic epilepsy, seizures cannot be controlled in as many as 25% patients, and therefore there is a need for new therapeutic approaches². At the same time, there is growing awareness that the development of new therapies has slowed, and to move toward new and more effective therapies, novel approaches to therapy discovery

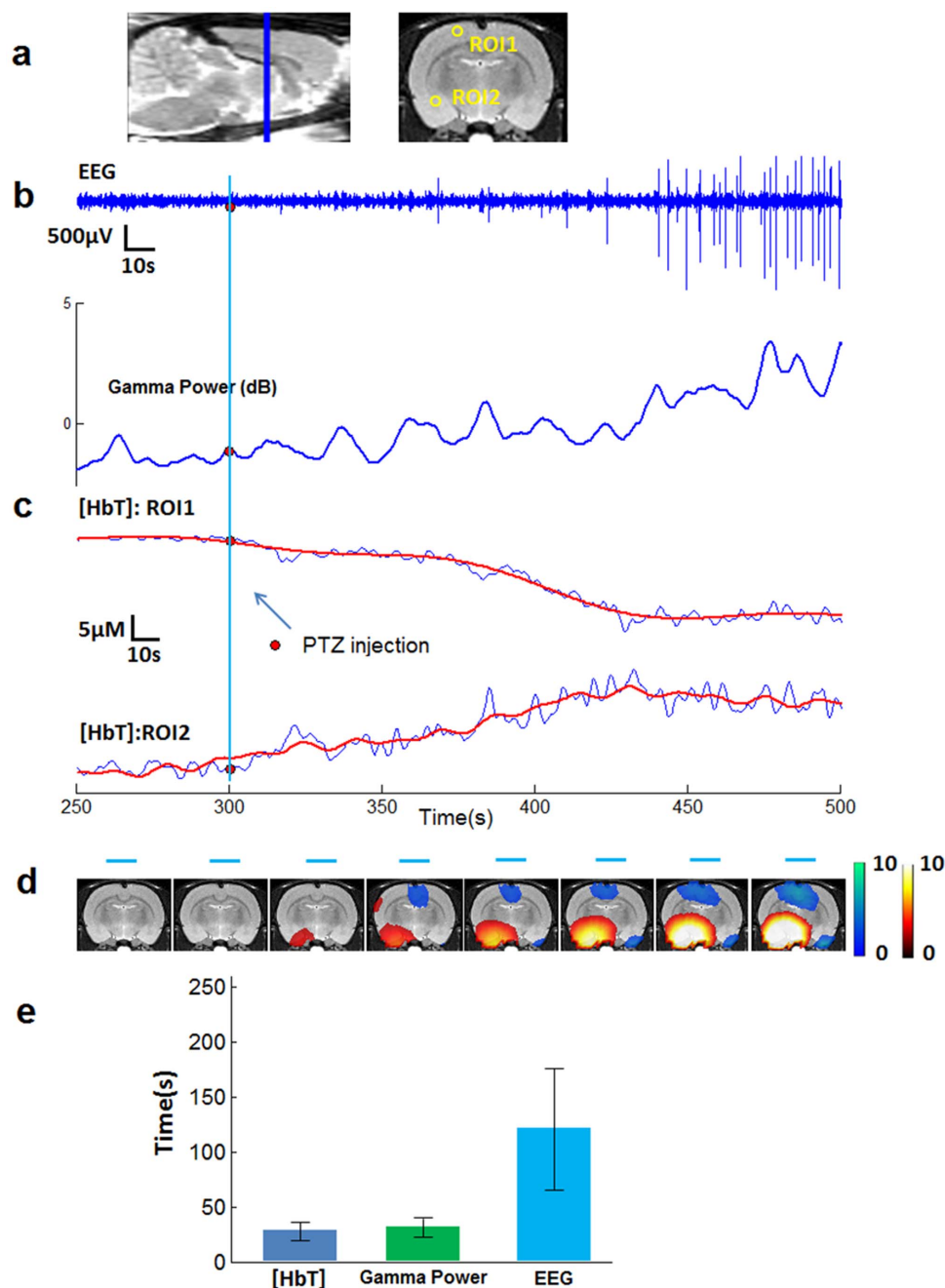


Figure 2 | Hemodynamic changes precede EEG seizure onset. (a) Locations of two ROIs, one from the motor cortex and the other from temple lobe, shown on a coronal slice (right). The sagittal plane (left) gives the position of the coronal slice. (b) EEG recording from electrode placed at ROI1 and its gamma power change. EEG seizure onset began about 3 minute after PTZ injection. EEG gamma power changes started much earlier than EEG spikes. (c) [HbT] changes (blue) with fitted curves (red) from two typical ROIs. Significant hemodynamic changes started 20 s after PTZ injection. (d) Activation map of HbT showing the evolution of hemodynamic distribution, superimposed on the MRI template. Negative activation (cool colors) means decreasing [HbT], while positive activation (warm colors) stands for increasing [HbT]. Blue lines specify the time period corresponding to each activation map. (b) and (c) share a same time line. (b) ~ (d) are results from rat #2. (e) Results from all experiments ($n = 9$, mean \pm s.d.) of the time lengths between PTZ injections and occurrence of EEG seizure onset, significant gamma power changes and significant hemodynamic changes.

are needed. A growing body of research indicates that controlling seizures may be possible by employing a seizure prevention closed-loop treatment strategy^{35,36}. For patients this would be a significant breakthrough as they would not be dependent on daily anticonvulsant treatment. Seizure prevention techniques could conceivably be coupled with treatment strategies aimed at interrupting the process before seizures evolve. Treatment would conceivably occur only when needed: on-demand and in advance of an impending seizure.

To develop seizure prevention/intervention models for a specific application, it is necessary to first establish that a pre-seizure state actually exists. The main finding of our experiments is the early changes during the transition from resting interictal state to ictal state involves spatiotemporal changes in hemodynamics, as well as IIEG gamma power, several minutes in advance of overt seizure spikes in local field potentials. Although the mechanisms of seizure generation are still unknown, there is evidence that measurable changes occur prior to seizures^{22,37}. Accumulated experimental evi-

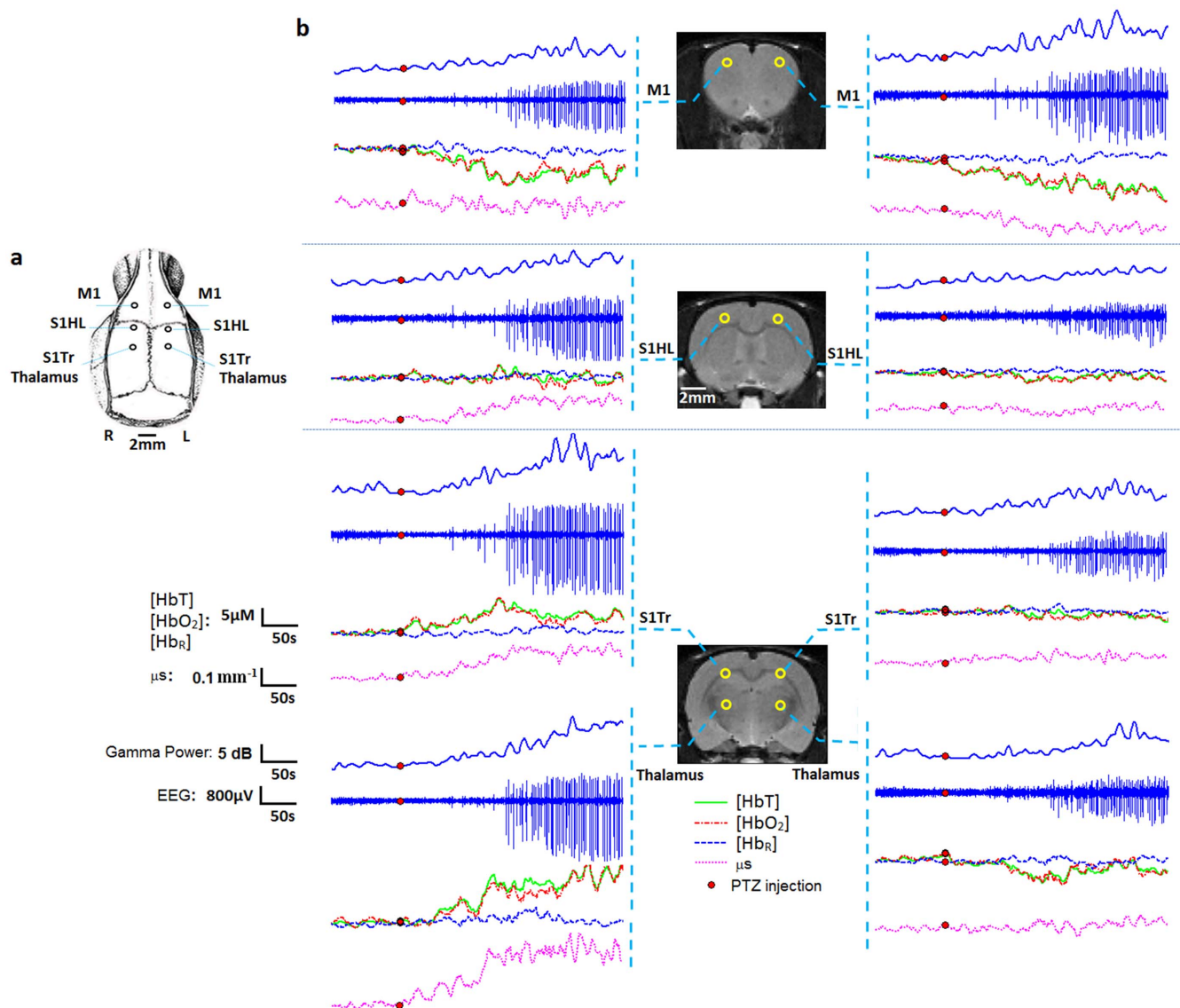


Figure 3 | Comparison between multisite recordings of IEEG signals, gamma power, hemoglobin concentrations and tissue scattering properties. (a) Schematic showing the locations of six holes inserted with eight EEG electrodes. (b) Three coronal MRI templates showing eight region of interest located on the left and right primary motor (M1) cortex, hind limb primary somatosensory (S1HL) cortex, somatosensory cortex trunk region (S1Tr) and anterior thalamus. For each region of interest, IEEG recordings and corresponding gamma powers, hemodynamic responses of [HbT], [HbO₂] and [Hb_R] and scattering coefficients (μ s) responding to the cellular volumes are shown. Results are from rat #2.

dences have suggested that HFOs in the gamma and fast gamma range (40 ~ 120 Hz) in IEEG recordings, are not only an electrical signature of focal epilepsy during seizure-free states, but may also play a causal role in the initiation of seizures⁶. Many neocortical seizures were preceded by a build-up of gamma power prior to seizures. On the other hand, works on animals and humans indicate that gamma band neuronal synchronization in electrophysiological recordings is closely related to the BOLD signal^{34,38}. In parallel to these evidences, our findings suggest that DOT can serve as an alternative technique to IEEG to detect preictal activities noninvasively.

Indeed anecdotal reports of preictal changes in brain hemodynamics have been reported with SPECT^{13,14}, fMRI¹⁵, and optical imaging²⁰. The dissociating hemodynamic changes from neural activities have been discussed in a review³⁹ with several hypotheses. One hypothesis is that such decoupling is due to the inability of scalp EEG or Electroencephalography (ECoG) to detect activities deep in the brain or high frequency local field potential activity. According to our experiment results, with multisite electrode recordings distributed

in several regions within the brain, such high frequency changes can be observed in some IEEG channels, and came together with the hemodynamic changes (Fig. 3b). Our findings of the concurrent optical scattering change also support another hypothesis that hemodynamic responses could be triggered by increased activities of glial cells. It has been shown that glial cells play a key role in neurometabolism and neurovascular coupling⁴⁰ and cell swelling and shrinkages alter the tissue density, thereby changing the scattering properties of brain tissues. Thus, glial cell volume changes, which could change tissue scattering properties but not detectable in neuronal activity, could induce the hemodynamic activities preceding neuronal activity. Such decoupling suggests that DOT can be more sensitive than IEEG recordings to detect subtle changes.

Generalized epilepsy is characterized by seizures with diffuse, bilateral cerebral involvement, and affects the entire forebrain including both hemispheres of the brain, in contrast to the focal seizures, which originate from focal brain regions and affect only a part of the brain at onset⁴¹. In generalized epilepsy multifocal

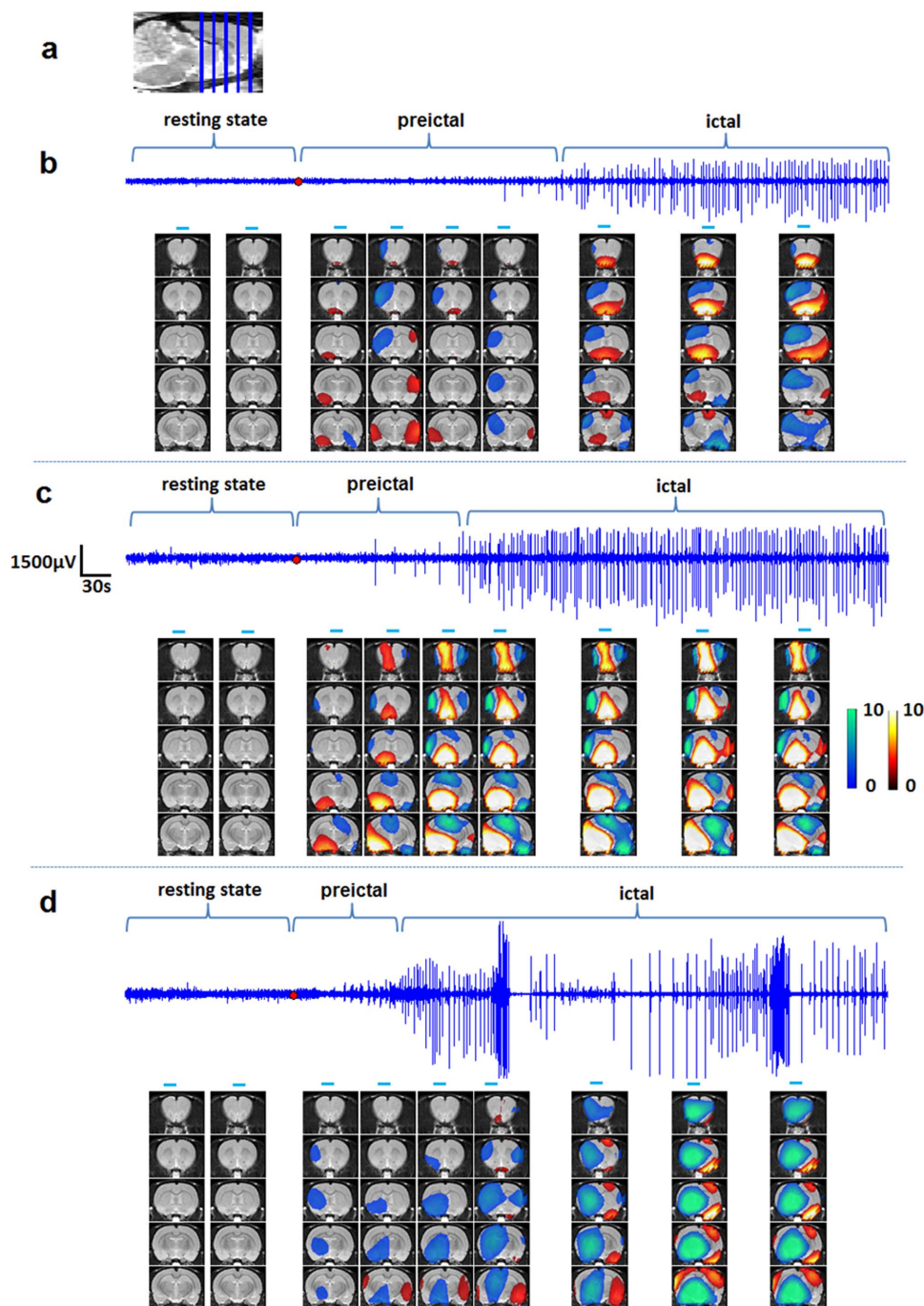


Figure 4 | Evolution of [HbT] prior to and during a PTZ induced seizure. (a) shows the positions of five coronal slices. (b), (c) and (d) are the results from three seizure experiments (rat #2, #3, and #4) with different seizure intensities. IEEG recordings and statistical activation maps depict [HbT].

neocortical regions have the potential to initiate a seizure. Networks or neuronal circuits involved in seizures include the seizure focus, the initiating circuit, the pathways of spread, and the modulatory centers⁴². It has been shown that the interaction between the cortex and several nuclei of the thalamus involved in the key circuit for discharges in the generalized seizures⁴³. As can be seen in Fig. 4, during early seizure onset, both the thalamus and bilateral cortex are activated, and as the seizure progresses, adjacent regions are progressively activated.

Despite different patterns of seizures and different origin locations, hemodynamic changes all developed from local regions involving bilateral cortex and thalamus to the larger area. These findings suggest that so-called “generalized” tonic-clonic seizures may be in

fact localized, at least during the early phase of seizure onset. Indeed, the concept of a cortical focus has also been previously discussed in other generalized seizure studies^{4,41,42}. The concept of focal cortical origins during generalized tonic-clonic seizures provides implications for understanding and treating this disorder in human patients, which may ultimately enable targeted therapies including neurostimulation, disconnection procedures, and novel pharmacological treatments directed at involved regions⁴.

In this study, we did not apply statistical group analysis as has been used in other studies^{3,4}. As shown in Fig. 4b–d, for the PTZ-induced generalized tonic-clonic seizures model, seizures can occur in a variety of IEEG manifestation, even with the same PTZ injection due to individual variation for each rat. Such changes in electrophysiology



accompany with hemodynamic change with distinct patterns in terms of both spatial and temporal distribution. Group analysis could potentially smooth or even remove subtle changes in certain areas.

Heterogeneous patterns of hemodynamic changes have been observed in our experiments. Studies of functional activation using optical techniques have shown the hemodynamic response in newborn infants³³ and a rat model¹⁸ to be highly variable. SPECT studies of both spontaneous secondarily generalized and electroconvulsive therapy-induced tonic-clonic seizures reported heterogeneous patterns of changes in CBF during seizures^{3,44}. In fMRI studies⁴⁵, a mixed pattern of focal increased and decreased BOLD activity has been shown in humans and animals during generalized seizures, and relationship between neuronal activity and BOLD signals may depend on brain region and state. One hypothesis is that preictal vasoconstriction surrounding the seizure focus could actively shunt blood to the ictal focus to prepare the focus for the impending dramatic increase in neuronal activity and metabolism¹⁸. However, as shown in Fig. 3, locations with either increase (left thalamus and S1Tr) or decrease (M1) of [HbO₂] all came with significant gamma power increase (t-test, $p < 0.05$) during the preictal period and spikes strong seizure during ictal period. Moreover, although it is well understood that the increase in CBF caused by the cerebral metabolic rate of oxygen (CMRO₂) and glucose comes with increased neuronal activity, it is still not clear if such CBF increase can satisfy local metabolic demands³⁹. Depending on the interplay between hemodynamics and metabolism, increase of [HbO₂] could arise when the relative increase in CBF is more than the actual need of metabolism. On the other hand, decrease of [HbO₂] suggests an exceedingly high metabolic demand without appropriate compensatory blood flow especially around the seizure focus, rather than a decrease in neuronal activity^{45,46} (Fig. 4b–d).

While our study provides information for seizure dynamics, it does have several limitations that are worth noting and should be addressed through future investigation. First, the imaging domain should cover the whole brain. Although a large portion of the rat brain was included in our current study, we cannot exclude possibly important changes in more posterior brain regions. For example, much previous work supports an important role for the brainstem in generalized seizures both in human patients and animals^{3,4,46}. Second, the studies should be done continuously and over weeks in freely moving animals. Also, although the PTZ animal model serves the role of a good proof-of-concept model to test our primary hypothesis, future studies should be focused on chronic epilepsy via an animal model with intermittent spontaneous seizures. Third, anatomical information from MRI should be used in the future study. Earlier studies have shown that incorporating subject-specific structural priors into the DOT reconstruction process could improve the location and quantitative accuracy in human head⁴⁷ or breast imaging⁴⁸. Besides, subject-specific wearable interface can be built with the MRI-derived anatomical information, and applied to freely moving rats to facilitate the study of chronic epilepsy with spontaneous seizures.

In summary, through the use of a PTZ-induced generalized seizure model, we were able to investigate early seizure initiation and onset as well as seizure propagation patterns. Such studies are essential to understanding ictogenesis and guiding seizure prevention strategies thereof. To this end, DOT offers an opportunity for observing global hemodynamic changes related to neural activities and for capturing the genesis and distribution of generalized seizures. The possibility of seizure prediction, most importantly, has given hope for new warning and therapeutic devices for individuals who cannot be successfully treated with current therapies.

Methods

All experimental procedures were approved by IACUC committee at the University of Florida.

Animal model. Eleven adult male Sprague-Dawley rats (Harlan Labs, Indianapolis) weighing 360–450 g were used for the *in vivo* experiments. Animals were housed in pairs in a controlled environment (12: h light/dark cycle; food and water ad lib).

Rats were anaesthetized with i.p. Urethane (1 g/kg, Sigma-Aldrich, Inc.). The generalized tonic-clonic seizures were induced by i.p. 130 mg/kg of PTZ (Sigma-Aldrich, Inc.)⁴⁹. PTZ is the most commonly used GABA_A receptor antagonist used to induce absence-like seizures. With low doses (100 mg/kg IP) seizures develop within 20 minutes after application. PTZ induces all four behavioral phenomena: freezing, myoclonic twitches, clonic seizures, and tonic-clonic seizures. Tonic-clonic seizures are believed to represent generalized seizures. Although PTZ exerts its action mostly via the t-butyl-bicyclo-phosphorothionate site of the GABA_A receptor⁵⁰, metabolic [14C] 2-deoxyglucose studies demonstrate that there is an uptake or metabolic activation in the motor and limbic cortex after PTZ in rat pups and in adult rats, a redistribution of glucose uptake from the cortex and hippocampus to the midbrain, brainstem, hypothalamus, and septum in adult rats⁵¹. In young rats (<P21), after subconvulsive doses of PTZ, *c-fos* was expressed in the medial thalamus, cortex, and globus pallidus. Occurrence of clonic seizures induced *c-fos* immunoreactivity in the cortex, thalamus, hypothalamus, and brainstem. After clonic seizures, *c-fos* was found also in the striatum, nucleus accumbens, brainstem, and hippocampus⁴⁹.

Time-locked IEEG/DOT were performed continuously for 30 minutes surrounding each PTZ or saline (control experiments) injection, 5 minutes before injection for the resting state recording, and then 25 minutes after injection for seizure recording. A total of 9/11 rats were received PTZ, while 2/11 were used as age-matched sham controls.

Electroencephalography. Continuous time-locked IEEG recordings were used to confirm the occurrence of seizures. In eight of eleven rats (two rats for control experiments; six rats for seizure experiments, including rats #1, #5 ~ 9 listed in the supplementary Fig. S1 and Table S1), two electrodes were placed in the bilateral frontal cortices (bregma coordinates: AP: 3 mm; ML: ±2.5 mm; DV: 1.5 mm)⁵² through two holes drilled on the skull. To monitor and verify the local field potentials, multisite IEEGs were recorded in other three rats (rats #2 ~ 4). In these experiments, eight microwire recording electrodes (50 μm polyimide insulated tungsten microwire) were implanted through six holes to eight typical bilateral locations on M1, S1HL, S1Tr, and anterior thalamic regions: M1(AP: 3 mm; ML: ±2.5 mm; DV: 1.5 mm), S1HL(AP: 0 mm; ML: ±2.5 mm; DV: 1.5 mm), S1Tr(AP: -3 mm; ML: ±2.5 mm; DV: 1.5 mm), and Thalamus(AP: -3 mm; ML: ±2.5 mm; DV: 5.5 mm). Positions of holes and electrodes are shown in Fig. 3. Electrodes for ipsilateral S1Tr and Thalamus were placed through a same hole since they share same perpendicular location. Electrodes were secured using tissue glue. One stainless steel screw electrode was implanted as a reference electrode into the midline occipital bone. Local field potentials were obtained in differential mode by a neural recording system (RZ5, Tucker-Davis Technologies, Inc.) at a sampling rate of 50 kHz and filtered from 0.5 to 6 kHz. A notch filter was used to remove 60 Hz power line interference. Electrocardiogram was also measured to monitor heart rate through one channel of this recording system. IEEG data was down sampled from 50 kHz to 600 Hz and then band-pass filtered from 2 to 200 Hz. The short-time Fourier transform was performed for time-frequency power spectrum density (PSD) analysis using Welch's method with a moving window of 6.8 s and 90% overlap. To quantify the level of activity in the Gamma frequency (80 ~ 120 Hz), which is considered closely related with the initiation of seizures⁶, IEEG spectral-band power was calculated by integration of power spectrum within that range. To determine the start of significant change in gamma power, t-test was performed on each IEEG channel by comparing gamma power in 30-second moving window with 80% overlap to the resting state, with the null hypothesis of none IEEG power change at a significant threshold of $p < 0.05$.

Defining generalized seizure onsets. Typical methods to identify the seizure onsets with IEEG are monitoring the appearance of epileptiform IEEG with characteristic of high-amplitude or fast activities^{53,54}. The start of seizure onset can be determined when several number of IEEG channels satisfy such feature. The epileptic seizures induced with PTZ in our experiments are generalized tonic-clonic seizures, featured with continuous high-amplitude, high-frequency spike and wave activity affecting both cerebral hemispheres (covering all IEEG electrode positions in our experiment) from the beginning of the seizure⁴⁹. Therefore, to eliminate any confusion regarding the onset of the seizure, only the beginning of continuous high-amplitude and high-frequency spikes observed in all IEEG channels was considered as the onset of generalized seizures, although it could miss some scattered abnormal electrophysiological changes in certain channels that occur earlier. Based on this standard, seizure onset was identified by visual analysis of electrographic morphology and its corresponding PSD for each rat PTZ experiment.

DOT experiment and image reconstruction. We used a fast multispectral DOT system for optical signal recording, as described in detail previously⁵⁵. The system is schematically illustrated in Fig. 5. Briefly, the system performs continuous-wave measurements using 144 light emitting diodes (LEDs) as the excitation sources through a time multiplexing approach and highly sensitive photodetectors working in parallel for light detection. Forty-eight optical source/detector pairs were distributed equally along a cylindrical interface, sequentially shining light to the rat head and collecting the diffused scattered light. To ensure good contact and optical coupling between the optical fibers/skin, the gap between the head and the fiber interface was filled with Intralipid/India ink solution. This DOT system allows a full set of 3-D data

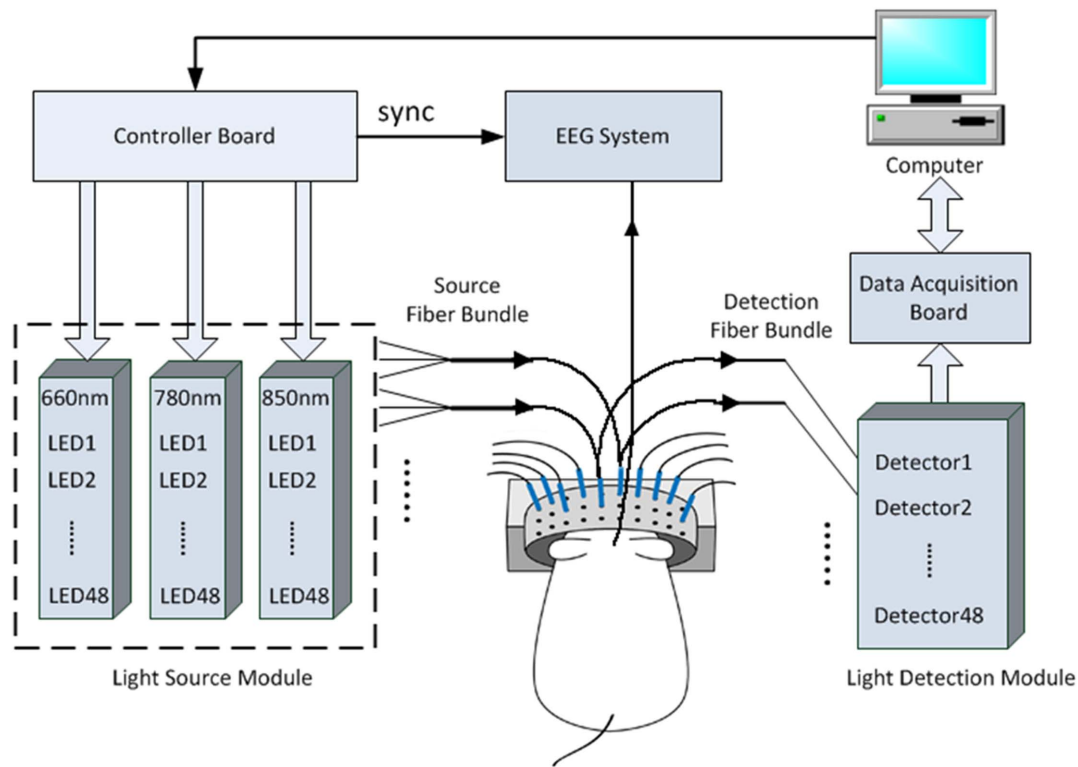


Figure 5 | Real time multispectral DOT system for imaging dynamics of generalized seizure.

collection at 3 NIR wavelengths (660, 780, and 850 nm) for whole brain imaging in 14.4 Hz. The data acquisition for both DOT and IEEG recording was synchronized through a controller board (PCI-7811R, NI).

In order to provide reliable data for the image reconstruction and analysis, noise should be firstly considered and reduced. Basically, instrumental noise, experimental errors and systemic physiological artifacts compose the three major sources of noise⁵⁶. A recent system upgrade to DAQ boards (NI-6358) with higher sampling rate allowed an online signal averaging of 100 times for one set of sampling data, which significantly suppressed the random noise as a large part of instrumental noise. A temporal low-pass filter (1 Hz) was applied to attenuate physiological artifacts from movement, heart beating, and breathing^{22,57}.

After the multispectral signals are collected, an effective model-based reconstruction algorithm is critical for accurate image reconstruction in DOT brain imaging. Our DOT algorithm is based on the finite element solution to the following photon diffusion equation coupled with Robin boundary conditions:

$$\nabla \cdot D(r) \nabla \Phi(r) - \mu_a(r) \Phi(r) = -S(r) \quad (1)$$

$$-D(r) \nabla \Phi_n = \alpha \Phi \quad (2)$$

where $\Phi(r)$ is the photon density, α is a coefficient related to the internal reflection at the boundary, $\mu_a(r)$ are the diffusion and absorption coefficients, and $S(r)$ is the source term. The diffusion coefficient can be written as $D(r) = 1/(\mu_a(r) + \mu'_s(r))$, where $\mu'_s(r)$ is the reduced scattering coefficient. The objective of the DOT reconstruction algorithm is to recover $\mu_a(r)$ and $\mu'_s(r)$ at all positions inside the computational domain, achieved through a regularized Newton's method to update an initial optical property distribution iteratively in order to minimize a weighted sum of the squared difference between computed and measured optical data along its boundary. A calibration method was applied to reduce the errors caused by the use of different source/detection intensities/positions and the system hardware⁵⁵.

Although the continuous wave DOT is theoretically challenged by Arridge and Lionheart⁵⁸, claiming that simultaneous unique recovery of $\mu_a(r)$ and $\mu'_s(r)$ cannot be achieved from CW data, our approach is different due to several factors⁵⁹. First, regularization techniques were used to solve the ill-posed inverse problem during reconstruction. The core procedure in our reconstruction algorithms is to iteratively solve the following regularized matrix equation:

$$(J^T J + \lambda I) \Delta q = J^T (\Phi^{(m)} - \Phi^{(c)}) \quad (3)$$

where $\Phi^{(m)}$ and $\Phi^{(c)}$ are the measured and computed photon density; J is the Jacobian matrix consisting of the derivatives of Φ with respect to D and μ_a at the boundary measurement sites; I is the identity matrix, and λ is the regularization parameter determined by combined Marquardt and Tikhonov regularization schemes ($\lambda = 0.5$ was used in this study. we have found that the quality of inversion was not sensitive to

the choice of this parameter). $\Delta q = (\Delta D_1, \Delta D_2, \dots, \Delta D_{N_s}, \Delta \mu_{a,1}, \Delta \mu_{a,2}, \dots, \Delta \mu_{a,N})^T$ is the update vector for the optical property profiles, where N is the total number of nodes in the finite element mesh. Second, an optimization procedure was applied to search for the best parameter set of initial $\mu_a(r)$ and $\mu'_s(r)$ based on *a priori* information (biologically feasible ranges of these initial parameters). The optimization procedure seeks best parameter space in the vicinity of the exact one and has allowed the minimization of the object function to be confined in a $(\mu_a(r), \mu'_s(r))$ parameter subspace that is close to the exact solution. Using extensive laboratory experiments, we have demonstrated that the scattering and absorption coefficients can be distinguished and the solution is unique in many practical scenarios⁶⁰. These facts have also been corroborated by other researchers⁶¹.

A three-dimensional cylindrical FE mesh, consisting of 22,764 tetrahedron elements, was used for the image reconstruction. To efficiently process a large amount of data containing thousands of time points for one set of experiment, a GPU (graphic processing units) based parallel code⁶² was implemented using CUDA programming model (NVIDIA), allowing the time consuming image reconstructions for one set of experiment to be processed within one day.

DOT analysis and rat atlas registration. Assuming oxy- and deoxy-hemoglobin (HbO_2 and Hb_R) are the two major chromophores in the rat brain, the absorption coefficients at 660 nm, 780 nm and 850 nm were used to obtain $[\text{HbO}_2]$ and $[\text{Hb}_R]$ using the Beer-Lambert law⁶³ and least square fitting through pseudo inverse matrix calculation. The concentration of total hemoglobin (HbT) was then calculated by summing up $[\text{HbO}_2]$ and $[\text{Hb}_R]$ which is proportional to CBV. $[\text{HbT}]$ has been suggested to map cerebral activity in NIRS for its better spatial specificity than $[\text{HbO}_2]$ or $[\text{Hb}_R]$ ⁶⁴. Activation maps were generated by tracking the change of $[\text{HbT}]$ that exceeded significant threshold, because HbT contains the information of both $[\text{HbO}_2]$ and $[\text{Hb}_R]$ and reflects the local CBV. For statistical analysis, thirty seconds (432 images) consecutive $[\text{HbT}]$ images preceding PTZ injection were chosen as a baseline period to which all analysis periods were compared. Several time series images, each covering a 10 seconds time bin (144 images), were selected from the interictal, pre-seizure, and seizure periods. A t-test was performed by comparing each time bin to baseline using a voxel wise 2-sample t-test, with a significant threshold of $p < 0.05$. Activation maps were then overlaid with template MRI images obtained from the Karolinska rat atlas (<http://expmr.ki.se/research/ratatlas.jsp>) for anatomical guidance.

Activation maps were visualized through the following procedures. First, Amira (Visage Imaging, Inc.) was used to detect the brain surface from the MRI template and generated a brain mask. Then, DOT image coordinate was aligned with the atlas coordinate by comparing the measured bregma position from experiments and its according position in the atlas. Next, DOT images within the brain mask were interpolated to each voxels (1 mm^3) in the atlas using Matlab. Results were converted and stored in NIFTI format, which were visualized with MRIcron (<http://www.mricro.com/>).



1. Neligan, A., Hauser, W. & Sander, J. The epidemiology of the epilepsies. *Handbook of clinical neurology* **107**, 113 (2012).
2. Jacobs, M. P. *et al.* Curing epilepsy: progress and future directions. *Epilepsy Behav.* **14**, 438–445 (2009).
3. Blumenfeld, H. *et al.* Cortical and subcortical networks in human secondarily generalized tonic–clonic seizures. *Brain* **132**, 999–1012 (2009).
4. DeSalvo, M. N. *et al.* Focal BOLD fMRI changes in bicuculline-induced tonic–clonic seizures in the rat. *Neuroimage* **50**, 902–909 (2010).
5. Nei, M. & Hays, R. Sudden unexpected death in epilepsy. *Curr. Neurol. Neurosci. Rep.* **10**, 319–326 (2010).
6. Stacey, W., Le Van Quyen, M., Mormann, F. & Schulze-Bonhage, A. What is the present-day EEG evidence for a preictal state? *Epilepsy Res.* **97**, 243–251 (2011).
7. Nelson, R. *et al.* Detection of high frequency oscillations with Teager energy in an animal model of limbic epilepsy. in *Engineering in Medicine and Biology Society, 2006. EMBS'06. 28th Annual International Conference of the IEEE.* 2578–2580 (IEEE).
8. Carney, P. R., Myers, S. & Geyer, J. D. Seizure prediction: methods. *Epilepsy Behav.* **22 Suppl 1**, S94–101, doi:10.1016/j.yebeh.2011.09.001 (2011).
9. Mormann, F., Andrzejak, R. G., Elger, C. E. & Lehnertz, K. Seizure prediction: the long and winding road. *Brain* **130**, 314–333, doi:10.1093/brain/awl241 (2007).
10. Frei, M. G. *et al.* Controversies in epilepsy: debates held during the Fourth International Workshop on Seizure Prediction. *Epilepsy Behav.* **19**, 4–16 (2010).
11. Zaveri, H. P., Frei, M. G., Arthurs, S. & Osorio, I. Seizure prediction: The Fourth International Workshop. *Epilepsy Behav.* **19**, 1–3 (2010).
12. Lehnertz, K. & Litt, B. The first international collaborative workshop on seizure prediction: summary and data description. *Clin. Neurophysiol.* **116**, 493–505 (2005).
13. Baumgartner, C. *et al.* Preictal SPECT in temporal lobe epilepsy: regional cerebral blood flow is increased prior to electroencephalography-seizure onset. *J. Nucl. Med.* **39**, 978 (1998).
14. Hong, S. B. *et al.* Preictal versus ictal injection of radiotracer for SPECT study in partial epilepsy: SISCOM. *Seizure* **17**, 383–386 (2008).
15. Federico, P., Abbott, D. F., Briellmann, R. S., Harvey, A. S. & Jackson, G. D. Functional MRI of the pre-ictal state. *Brain* **128**, 1811–1817 (2005).
16. Donaire, A. *et al.* Identifying the structures involved in seizure generation using sequential analysis of ictal-fMRI data. *Neuroimage* **47**, 173–183 (2009).
17. Grinvald, A. Imaging input and output dynamics of neocortical networks in vivo: exciting times ahead. *Proc. Natl. Acad. Sci. U. S. A.* **102**, 14125–14126 (2005).
18. Zhao, M. *et al.* Preictal and ictal neurovascular and metabolic coupling surrounding a seizure focus. *J. Neurosci.* **31**, 13292–13300 (2011).
19. Haglund, M. M. Optical imaging of visual cortex epileptic foci and propagation pathways. *Epilepsia* **53**, 87–97 (2012).
20. Zhao, M. *et al.* Focal increases in perfusion and decreases in hemoglobin oxygenation precede seizure onset in spontaneous human epilepsy. *Epilepsia* **48**, 2059–2067 (2007).
21. Nguyen, D. K. *et al.* Non-invasive continuous EEG-fNIRS recording of temporal lobe seizures. *Epilepsy Res.* (2011).
22. Osharina, V., Ponchel, E., Aarabi, A., Grebe, R. & Wallois, F. Local haemodynamic changes preceding interictal spikes: a simultaneous electrocorticography (ECoG) and near-infrared spectroscopy (NIRS) analysis in rats. *Neuroimage* **50**, 600–607 (2010).
23. Irani, F., Platek, S. M., Bunce, S., Ruocco, A. C. & Chute, D. Functional near infrared spectroscopy (fNIRS): an emerging neuroimaging technology with important applications for the study of brain disorders. *Clin Neurophysiol* **21**, 9–37 (2007).
24. Li, C., Zhao, H., Anderson, B. & Jiang, H. Multispectral breast imaging using a ten-wavelength, 64 × 64 source/detector channels silicon photodiode-based diffuse optical tomography system. *Med. Phys.* **33**, 627, doi:10.1118/1.2171508 (2006).
25. Yuan, Z., Zhang, Q., Sobel, E. & Jiang, H. Three-dimensional diffuse optical tomography of osteoarthritis: initial results in the finger joints. *J. Biomed. Opt.* **12**, 034001-034001-034011 (2007).
26. Culver, J. P. *et al.* Diffuse optical tomography of cerebral blood flow, oxygenation, and metabolism in rat during focal ischemia. *J. Cereb. Blood Flow Metab.* **23**, 911–924, doi:10.1097/01.WCB.0000076703.71231.BB (2003).
27. Graves, E. E., Ripoll, J., Weissleder, R. & Ntzachristos, V. A submillimeter resolution fluorescence molecular imaging system for small animal imaging. *Med. Phys.* **30**, 901 (2003).
28. Gibson, A. *et al.* Three-dimensional whole-head optical tomography of passive motor evoked responses in the neonate. *Neuroimage* **30**, 521–528 (2006).
29. White, B. R. & Culver, J. P. Phase-encoded retinotopy as an evaluation of diffuse optical neuroimaging. *Neuroimage* **49**, 568–577, doi:10.1016/j.neuroimage.2009.07.023 (2010).
30. Habermehl, C., Schmitz, C. H. & Steinbrink, J. Contrast enhanced high-resolution diffuse optical tomography of the human brain using ICG. *Opt. Express* **19**, 18636–18644, doi:10.1364/OE.19.018636 (2011).
31. Zhou, C. *et al.* Diffuse optical correlation tomography of cerebral blood flow during cortical spreading depression in rat brain. *Opt. Express* **14**, 1125–1144 (2006).
32. Gallagher, A. *et al.* Non-invasive pre-surgical investigation of a 10 year-old epileptic boy using simultaneous EEG–NIRS. *Seizure* **17**, 576–582 (2008).
33. Cooper, R. *et al.* Transient haemodynamic events in neurologically compromised infants: A simultaneous EEG and diffuse optical imaging study. *Neuroimage* **55**, 1610–1616 (2011).
34. Niessing, J. *et al.* Hemodynamic signals correlate tightly with synchronized gamma oscillations. *Science* **309**, 948–951 (2005).
35. Fisher, R. S. Therapeutic devices for epilepsy. *Ann. Neurol.* **71**, 157–168 (2012).
36. Berényi, A., Belluscio, M., Mao, D. & Buzsáki, G. Closed-loop control of epilepsy by transcranial electrical stimulation. *Science* **337**, 735–737 (2012).
37. Mormann, F. *et al.* On the predictability of epileptic seizures. *Clin. Neurophysiol.* **116**, 569–587 (2005).
38. Scheeringa, R. *et al.* Neuronal dynamics underlying high- and low-frequency EEG oscillations contribute independently to the human BOLD signal. *Neuron* **69**, 572–583 (2011).
39. Schwartz, T. H., Hong, S. B., Bagshaw, A. P., Chauvel, P. & Bénar, C. G. Preictal changes in cerebral haemodynamics: review of findings and insights from intracerebral EEG. *Epilepsy Res.* **97**, 252–266 (2011).
40. Figley, C. R. & Stroman, P. W. The role (s) of astrocytes and astrocyte activity in neurometabolism, neurovascular coupling, and the production of functional neuroimaging signals. *Eur. J. Neurosci.* **33**, 577–588 (2011).
41. Holmes, M. D., Brown, M. & Tucker, D. M. Are “generalized” seizures truly generalized? Evidence of localized mesial frontal and frontopolar discharges in absence. *Epilepsia* **45**, 1568–1579 (2004).
42. Bertram, E. H. Neuronal circuits in epilepsy: Do they matter? *Exp. Neurol.* (2012).
43. Avoli, M. & Gloor, P. Interaction of cortex and thalamus in spike and wave discharges of feline generalized penicillin epilepsy. *Exp. Neurol.* **76**, 196–217 (1982).
44. McNally, K. A. & Blumenfeld, H. Focal network involvement in generalized seizures: new insights from electroconvulsive therapy. *Epilepsy Behav.* **5**, 3–12 (2004).
45. Schridde, U. *et al.* Negative BOLD with large increases in neuronal activity. *Cereb. Cortex* **18**, 1814–1827 (2008).
46. Brevard, M. E., Kulkarni, P., King, J. A. & Ferris, C. F. Imaging the Neural Substrates Involved in the Genesis of Pentylentetrazol-induced Seizures. *Epilepsia* **47**, 745–754 (2006).
47. Custo, A. *et al.* Anatomical atlas-guided diffuse optical tomography of brain activation. *Neuroimage* **49**, 561–567 (2010).
48. Yalavarthy, P. K. *et al.* Structural information within regularization matrices improves near infrared diffuse optical tomography. *Opt. Express* **15**, 8043–8058 (2007).
49. André, V., Pineau, N., Motte, J. E., Marescaux, C. & Nehlig, A. Mapping of neuronal networks underlying generalized seizures induced by increasing doses of pentylentetrazol in the immature and adult rat: a c-Fos immunohistochemical study. *Eur. J. Neurosci.* **10**, 2094–2106 (1998).
50. Olsen, R. W. The GABA postsynaptic membrane receptor-ionophore complex. *Mol. Cell. Biochem.* **39**, 261–279 (1981).
51. Nehlig, A., Vergnes, M., Marescaux, C. & Boyet, S. *Generalized Non-Convulsive Epilepsy: Focus on GABA-B Receptors* 141–153 (Springer, 1992).
52. Paxinos, G. & Watson, C. *The rat brain in stereotaxic coordinates.* (Academic press, 2007).
53. Makiranta, M. *et al.* BOLD signal increase precedes EEG spike activity—a dynamic penicillin induced focal epilepsy in deep anesthesia. *Neuroimage* **27**, 715–724, doi:10.1016/j.neuroimage.2005.05.025 (2005).
54. Schindler, K., Leung, H., Elger, C. E. & Lehnertz, K. Assessing seizure dynamics by analysing the correlation structure of multichannel intracranial EEG. *Brain* **130**, 65–77, doi:10.1093/brain/awl304 (2007).
55. Yang, J., Zhang, T., Yang, H. & Jiang, H. Fast multispectral diffuse optical tomography system for in vivo three-dimensional imaging of seizure dynamics. *Appl. Opt.* **51**, 3461–3469 (2012).
56. Huppert, T. J., Diamond, S. G., Franceschini, M. A. & Boas, D. A. HomER: a review of time-series analysis methods for near-infrared spectroscopy of the brain. *Appl. Opt.* **48**, D280–D298 (2009).
57. Roche-Labarbe, N. *et al.* NIRS-measured oxy- and deoxyhemoglobin changes associated with EEG spike-and-wave discharges in a genetic model of absence epilepsy: The GAERS. *Epilepsia* **51**, 1374–1384 (2010).
58. Arridge, S. R. & Lionheart, W. R. Nonuniqueness in diffusion-based optical tomography. *Opt. Lett.* **23**, 882–884 (1998).
59. Jiang, H. *Diffuse Optical Tomography: Principles and Applications.* (CRC Press, 2010).
60. Xu, Y., Gu, X., Khan, T. & Jiang, H. Absorption and scattering images of heterogeneous scattering media can be simultaneously reconstructed by use of dc data. *Appl. Opt.* **41**, 5427–5437 (2002).
61. Harrach, B. On uniqueness in diffuse optical tomography. *Inverse Probl* **25**, 055010 (2009).
62. Zhang, T. & Jiang, H. *Accelerating finite-element-based 3D optical imaging reconstruction by graphic processing units.* in *Biomedical Optics.* (Optical Society of America, 2012).
63. Bluestone, A. Y., Stewart, M., Lasker, J., Abdoulaev, G. S. & Hielscher, A. H. Three-dimensional optical tomographic brain imaging in small animals, part 1: hypercapnia. *J. Biomed. Opt.* **9**, 1046 (2004).
64. Gagnon, L. *et al.* Quantification of the cortical contribution to the NIRS signal over the motor cortex using concurrent NIRS-fMRI measurements. *Neuroimage* (2012).

Acknowledgments

This research was supported in part by an NIH grant (R01 NS069848), the J. Crayton Pruitt Family and the B.J. and Eve Wilder endowment funds.



Author contributions

T.Z. developed the imaging system, designed and performed experiments, analyzed data and wrote the paper; J.Z. designed and performed experiments; R.J. performed experiments; H.Y. helped system building; P.R.C. guided the experimental design, data analysis, and wrote the paper; H.J. directed the study and wrote the paper.

Additional information

Supplementary information accompanies this paper at <http://www.nature.com/scientificreports>

Competing financial interests: The authors declare no competing financial interests.

How to cite this article: Zhang, T. *et al.* Pre-seizure state identified by diffuse optical tomography. *Sci. Rep.* 4, 3798; DOI:10.1038/srep03798 (2014).



This work is licensed under a Creative Commons Attribution-NonCommercial-NoDerivs 3.0 Unported license. To view a copy of this license, visit <http://creativecommons.org/licenses/by-nc-nd/3.0>